

# COMPUTATION OF LIMIT CYCLE OSCILLATIONS AND THEIR STABILITIES IN NONLINEAR AEROELASTIC SYSTEMS USING HARMONIC BALANCE METHODS

Michael McGurk<sup>1</sup> and Jie Yuan<sup>1</sup>

<sup>1</sup>Aerospace Centre of Excellence  
University of Strathclyde, Glasgow, G1 1XQ, UK  
michael.mcgurk@strath.ac.uk  
jie.yuan@strath.ac.uk

**Keywords:** Aeroelasticity, Flutter, Harmonic Balance Method, Freeplay Nonlinearity, Numerical Continuation, Limit Cycle Oscillations

**Abstract:** Understanding the aeroelastic behaviour of aerospace systems is critical in aircraft design. The presence of structural nonlinearities can have a significant impact on these behaviours causing the onset of Limit Cycle Oscillations (LCO) and shifts in stability. Numerical continuation techniques have been implemented to detect and track the behaviour of these solutions. However, due to the complexity nonlinearities bring it is common practice to simplify the analysis to linear models that can underestimate the impact nonlinearities have. Nonlinear analysis tools can often be inefficient especially for large scale systems. Studies have shown that modelling nonlinear steady state vibrational behaviour in the frequency domain with Harmonic Balance Methods (HBM) can significantly improve the efficiency of nonlinear analysis. In this paper, the architecture of a HBM based continuation tool for analysis of nonlinear aeroelastic systems is presented. A simple 2D aerofoil case study featuring a freeplay nonlinearity is investigated with the tool and compared to state of the art alternative software that operate in the time domain. With this case study, it was shown that HBM provided both faster running times and less data storage requirements than alternative software. The devised HBM operated 11 times faster than MATCONT and 3 times faster than COCO for the same test case. Stability data obtained using Hill's method was also in agreement with COCO and time history comparisons. The significance of the freeplay nonlinearity is also demonstrated, shifting the safety margin of the design by 18% when compared to purely linear aeroelastic analysis.

## 1 INTRODUCTION

With the increasing integration of lightweight materials and complex systems, the study of nonlinearities in aerospace structures is becoming an important area of research. These nonlinearities can arise from various sources, from large structural deformation, unsteady aerodynamic force to friction and wear within structural joints [1]. The effects of these nonlinearities on dynamics and control can be very significant, changing flutter boundary in tiltrotor systems [2] and shifting the aerodynamic centre of certain wings effecting control [3]. However, the effects of nonlinearities are often neglected in analysis due to the added complexity and high computational cost [4], which greatly limits the design space of these aerospace systems. Bifurcation analysis has proven effective in revealing several stable and unstable solutions of nonlinear systems for a wide range of parameters. In aeroelastic systems, flutter and divergence speeds can be found at bifurcation points and solutions past can be further tracked through numerical

continuation. In particular, Limit Cycle Oscillations (LCO) of nonlinear aeroelastic systems can be detected, often revealing the maximum response of systems with major implications on structural fatigue [5]. LCO are characterised by undamped self-sustaining vibrations, which can be problematic in an aeroelastic context. The onset of LCO typically occurs at a specific type of bifurcation called a Hopf bifurcation [6]. It has been shown through both theory and experimentation that Hopf bifurcations occur at the flutter points of aeroelastic systems [7] [8]. The numerical continuation process uses previous solutions of the system and the equations of motion to accurately estimate the following solution with respect to a chosen continuation parameter. There is several methods mostly utilising a predictor to obtain a rough estimate then a corrector to improve the accuracy of the guess. Methods such as arclength and pseudoarclength continuation have proven effective at tracking solutions past turning points, revealing multiple behaviours for a system. Despite differences in existing bifurcation software, the most common tools are based on orthogonal collocation to track and model LCO [9] [10]. This is a time domain method in which a periodic orbit is divided into intervals, the unknown variables are represented by polynomials on each interval and the governing equations are collocated at Gauss points [11]. Orthogonal Collocation methods have been implemented in most common bifurcation software such as MATCONT [12], AUTO [13] and COCO [14]. While accurate, these methods are rarely employed for larger systems as considerable memory space is required leading to high computation expense [9].

Harmonic balance methods (HBM) provide a computationally less expensive alternative when identifying the maximum response of LCO. The periodic motion of LCO is approximated by Fourier series coefficients in the frequency domain. By carrying out analysis in the frequency domain only a set number of coefficients are required to be stored to characterise the response as opposed to a set of coordinates with corresponding time values in the time domain. Several previous studies [15] [16] have shown this method can achieve a good level of accuracy when compared to alternative methods such as the shooting method, whilst being much less expensive. In a comparison between HBM and orthogonal collocation on nonlinear mechanical systems, Karkar found HBM to have better convergence on certain systems and proved to be "very robust" [11]. Highlighted in the work however, is the lack of research in comparing HBM to current alternatives. Particularly in an aeroelastic context [9] [11] there is a low level of research. Most existing previous work is limited to low-harmonics or on forced non-autonomous systems [17]. The NLvib package [18] implements HBM but with a focus mainly on nonlinear mechanical systems and stability analysis is not included.

The aim of this work is to develop an efficient numerical tool to predict the maximum response in LCO and their stability for aeroelastic systems with different types of structural nonlinearities. The numerical tool will be based on HBM and numerical continuation techniques. Alternative Frequency Time scheme (AFT) will be implemented so different types of nonlinear forces can be evaluated in the time domain [19]. Considering the stability of LCO branches is important, as this reveals if states close to the branch settle at solutions away from the branch or towards it. Hill's method was selected to compute the stability of LCO [20]. This method calculates stability purely in the frequency domain, so is a proven practical choice when using HBM [21]. In this work, to demonstrate the capability of the tool, a case study involving a two degree-of-freedom aerofoil with a structural nonlinearity known as freeplay will be presented. A freeplay nonlinearity is selected as the behaviour can often occur in aging systems at joints and hinges [22]. Results from this study will be bench-marked by two other available software

namely MATCONT and COCO as well as being compared to time domain responses gathered from differential equation solvers. Both computational accuracy and efficiency will be compared and discussed. Finally, the impact of including the nonlinearity in the design of aerospace systems will be highlighted and compared to purely linear analysis.

## 2 METHODOLOGY

In this section the mathematical architecture of a numerical continuation tool based on HBM will be presented. In practice, the tool was constructed in MATLAB based around the methods laid out in Ref. [23]. First, set up of the general equations of motion will be shown and the linear analysis process is described. It will then be shown how HBM is utilised to conduct analysis in the frequency domain. The Nonlinear Frequency Domain Continuation Solver is then introduced, describing the constraints used to build the corrector. Prediction method and stability analysis via Hill's method are finally discussed.

### 2.1 General equation of motion

The methods laid out here are all based around mathematical models that can be arranged into the second order differential equation shown in Equation 1. Nonlinear aeroelastic systems can be arranged in this form assuming structural forces act to balance aerodynamic forces.

$$M\ddot{x} + D\dot{x} + Kx + q_{nl}f_{nl} = A\ddot{x} + B\dot{x} + Cx \quad (1)$$

Above,  $x$  denotes the system's degrees of freedom and  $M, D$  and  $K$  are the structural mass, damping and stiffness matrices respectively. Matrices  $A, B$  and  $C$  represent the encountered aerodynamic force, with size  $N \times N$  where  $N$  is the number of degrees of freedom of the system. Nonlinear function  $f_{nl}$  is used to represent different types of nonlinearities encountered in aeroelastic systems. The  $N \times 1$  vector  $q_{nl}$  is utilised to implement the nonlinear equations in the degrees of freedom they impact. The standard differential equation is rearranged into first order state Equation 2 as:

$$\dot{\mathbf{x}} = \mathbf{Q}\mathbf{x} + \mathbf{q}_n f_{nl} \quad (2)$$

Where:

$$\mathbf{x} = \begin{bmatrix} \dot{x} \\ x \end{bmatrix} \quad \mathbf{Q} = \begin{bmatrix} (M - A)^{-1}(B - D) & (M - A)^{-1}(C - K) \\ 0_{N \times N} & I_{N \times N} \end{bmatrix} \quad \mathbf{q}_n = \begin{bmatrix} -(M - A)^{-1}q_{nl} \\ 0_{N \times 1} \end{bmatrix}$$

Matrix  $\mathbf{Q}$  will be referred to as the linear matrix as it fully captures the linear behaviour of system. The system is arranged in this form so linear analysis can be conducted, determining the flutter point through the following procedure. Considering only the linear part of the system, Equation 2 can be written as the eigenvalue problem  $\dot{\mathbf{x}} - \mathbf{Q}\mathbf{x} = 0$ . Assuming a oscillatory response  $x = x_o e^{\psi t}$  the eigenvalue problem is written:

$$[\mathbf{Q} - \mathbf{I}\psi_{ij}] \phi = 0 \quad (3)$$

Where  $\psi_{ij}$  are eigenvalues in the conjugate pair

$$\psi_{ij} = -\zeta_{ij}\omega_{ij} \pm i\omega_{ij}\sqrt{1 - \zeta_{ij}^2} \quad (4)$$

where  $\omega_{ij}$  are the damped natural frequencies and  $\zeta_{ij}$  are the damping ratios. Matrix  $\phi$  contains the corresponding eigenvectors. Flutter is characterised by unstable negatively damped oscillations. From this definition it can be determined that if any of the real parts of Equation 4 is positive, the system is dynamically unstable [24].

Introducing nonlinearities into the analysis modifies this behaviour. In nonlinear systems, the loss of linear stability commonly results in the development of LCO at a hopf bifurcation point. Though linear analysis can identify where hopf bifurcation points occur, carrying out numerical continuation from a hopf point often show that LCO solutions can exist before the loss of linear stability. This was demonstrated in Ref. [4] that introducing structural nonlinearities into a tiltrotor system resulted LCO development in regions that appeared dynamically stable through purely linear analysis. The goal of the nonlinear analysis is to estimate the maximum vibrational response of an autonomous nonlinear system with respect to a selected continuation parameter  $\lambda$  and determine their stability. Through numerical continuation, the analysis should be able to detect vibrational solutions in regions linear analysis determines to be stable.

## 2.2 Harmonic Balance Methods

If it is assumed following a hopf bifurcation the dynamic response of the system is a LCO, the time response of  $x$  and  $\dot{x}$  can be represented using Fourier series. The unknowns can be expressed by multi-harmonic response and solved in frequency domain:

$$\begin{aligned} x(t) &= X_0 + \sum_{k=1}^l X_{k,s} \sin k\omega t + X_{k,c} \cos k\omega t \\ \dot{x}(t) &= \sum_{k=1}^l X_{k,s} \cos k\omega t - X_{k,c} \sin k\omega t \end{aligned} \quad (5)$$

Where  $l$  represents the harmonic order of the response and  $X_0$ ,  $X_{k,s}$  and  $X_{k,c}$  are Fourier coefficients. This assumed response is central to HBM, converting the system from the time domain to the frequency domain. The number of unknowns will become  $(2 \times l + 1) \times N$ . In addition to a set of Fourier coefficients, there is also natural frequency of the system  $\omega$  and the continuation parameter that can be any structural or aerodynamic parameters.

Nonlinear forces are commonly modelled as nonlinear time functions. Seeing as they are not linear functions of states or explicit functions of time, it is not possible to transform directly to the frequency domain [19]. However, the nonlinear force response is also be converted to the frequency domain through AFT procedure, which can be used to obtain  $F_0$ ,  $F_{k,s}$  and  $F_{k,c}$  as:

$$f_{nl}(t) = F_0 + \sum_{k=1}^l F_{k,s} \sin k\omega t + F_{k,c} \cos k\omega t \quad (6)$$

Predicted values of  $X_0$ ,  $X_{k,s}$ ,  $X_{k,c}$  and  $\omega$  are used in Equations 5 to obtain the time domain response over a period. The time domain nonlinear force response  $f_{nl}(t)$  is then found. A fast Fourier transform algorithm is used to estimate Fourier coefficients based on the time domain nonlinear force response. With the relationships described, the equation of motion shown in Equation 2 can be expressed into a set of algebraic residual equations, which are solved numerically using a Newton-Raphson solver [23].

## 2.3 Nonlinear Frequency Domain Continuation Solver

Figure 1 describes a basic outline of nonlinear solver in the frequency domain. The user must define a model in the form in Equation 2 and select the continuation parameter  $\lambda$ . Continuation is initiated based on an initial guess taken at a hopf bifurcation point. Hopf bifurcation points are

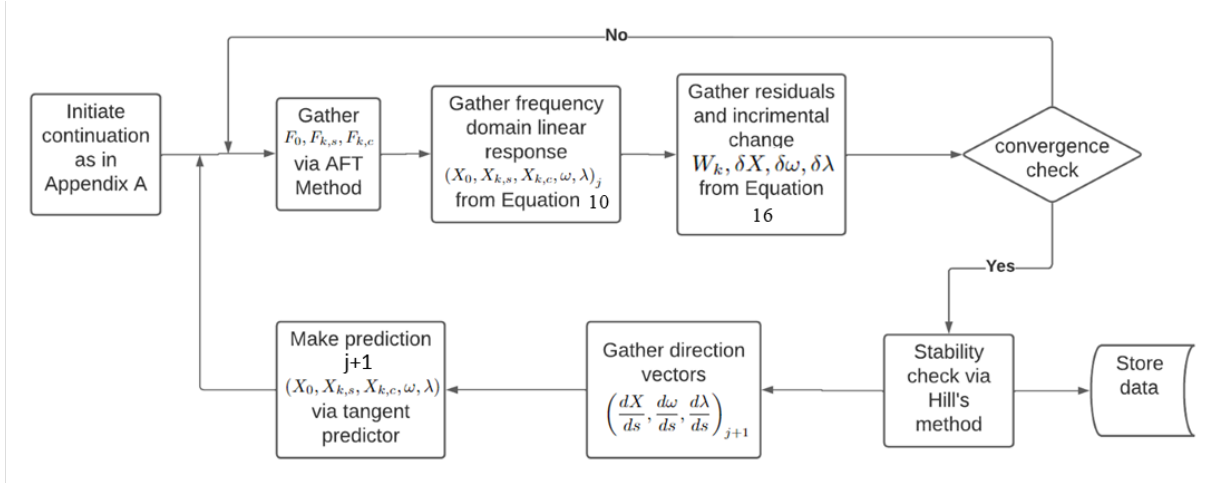


Figure 1: The architecture of the nonlinear continuation solver

identified through the linear analysis described in the previous section. Initial natural frequency  $\omega$  is taken as the imaginary part of the eigenvalues in Equation 4 with zero real part. A standard continuation procedure based on prediction-correction then takes place using a tangent predictor and correction via pseudo-arclength method. Stability of LCO is determined with Hill's stability technique, based on the Jacobean matrix of each converged solution. Each step will be detailed in the following. After correction, each converged solution is stored and the process is repeated until a user defined termination condition is met. Either a max/min  $\lambda$  or maximum number of points along the continuation.

### 2.3.1 Initiating Continuation

To commence the continuation process an initial guess at  $j = 0$  is made based on results from the linear analysis. The linear flutter point is taken as a hopf bifurcation point, where  $\omega$  and  $\lambda$  are the initial results. Typically at hopf bifurcation points, the amplitude of LCO is close to zero. So a small guess of  $X_{1,s}$  is used to solve a reduced version of System 15. In this reduced solver (shown in Appendix A.1),  $\lambda_0$  is treated as a known and  $\omega_0$  is taken as an initial guess. With no knowledge of other points, only residual Equations 11 can be solved, leaving  $l + 1$  equations and  $l + 2$  unknowns. To overcome this, a phase condition is set so  $X_{1,c} = 0$ . Once a converged solution is reached at  $j = 0$ , a small step is made in  $\lambda$  and the process is repeated for  $j = 1$ . With the initial two points converged, the first set of direction vectors can be calculated by obtaining arclength increment  $\delta s$  from Equation 7 and using finite difference method. Gathering direction vectors allows for the full Newton-Raphson solver to be implemented and arclength continuation to commence.

$$\delta s_{j+1} = \sqrt{(X_{j+1} - X_j)^T (X_{j+1} - X_j) + (\omega_{j+1} - \omega_j)^2 + (\lambda_{j+1} - \lambda_j)^2} \quad (7)$$

### 2.3.2 Linear Equation

In order to calculate the response of the nonlinear degree of freedom, the response of the linear part of the system  $\mathbf{x}_L$  is evaluated.  $\mathbf{x}_L$  represents the degrees of freedom of the system with the nonlinear degree of freedom  $x_{nl}$  removed. The linear and nonlinear parts of the system are solved separately so  $\mathbf{x}_L$  can be treated as a known when solving the nonlinear part, reducing the number of unknowns in the system. By removing the nonlinear degrees of freedom from Equation 2, the system can be rewritten as Equation 8. Equation 8 is treated as a non-autonomous

forced system, with the nonlinear degrees of freedom's impact acting as the forcing term.

$$\dot{\mathbf{x}}_L = (\mathbf{Q})_{p,p}\mathbf{x}_L + (\mathbf{Q})_{p,u}\dot{x}(t) + (\mathbf{Q})_{p,v}x(t) + (\mathbf{q}_n)_p f_{nl}(t) \quad (8)$$

It is assumed the linear response of the system is also in the shape described by Equation 5. Here,  $\bar{X}_0$ ,  $\bar{X}_{k,s}$  and  $\bar{X}_{k,c}$  are the linear Fourier coefficients. The subscript  $p$  denotes the linear degrees of freedom and  $v$  and  $u$  represent the nonlinear degree of freedom and nonlinear differential respectively. Equation 5 and the linear shape function are substituted into Equation 8. Performing Harmonic Balance by equating the constant, sine and cosine terms separately allows for System 9 to be constructed and hence, the linear Fourier coefficients to be obtained.

$$\begin{aligned} (\mathbf{Q})_{p,p} &= -(\mathbf{Q})_{p,v}\bar{X}_0 - (\mathbf{q}_n)_p F_0 \\ \begin{bmatrix} -(\mathbf{Q})_{p,p} & -k\omega\mathbf{I} \\ k\omega\mathbf{I} & -(\mathbf{Q})_{p,p} \end{bmatrix} \begin{bmatrix} \bar{X}_{k,s} \\ \bar{X}_{k,c} \end{bmatrix} &= \begin{bmatrix} -(\mathbf{Q})_{p,u}k\omega X_{k,c} + (\mathbf{Q})_{p,v}k\omega X_{k,s} \\ (\mathbf{Q})_{p,u}k\omega X_{k,s} + (\mathbf{Q})_{p,v}k\omega X_{k,c} \end{bmatrix} + \begin{bmatrix} (\mathbf{q}_n)_p F_{k,s} \\ (\mathbf{q}_n)_p F_{k,c} \end{bmatrix} \end{aligned} \quad (9)$$

### 2.3.3 Nonlinear equations

Once the Fourier's coefficients of the linear part are obtained, nonlinear section of Equation 2 gives the relationship as follows:

$$\ddot{x}_{nl}(t) = (\mathbf{Q})_{u,p}\mathbf{x}_L + (\mathbf{Q})_{u,u}\dot{x}_{nl}(t) + (\mathbf{Q})_{u,v}x_{nl}(t) + (\mathbf{q}_n)_u f_{nl}(t) \quad (10)$$

Substitution of Equations 5, 6 and the linear shape into the nonlinear relationship allows for three sets of residual equations to be derived. Harmonic balance is performed and the set of equations in System 11 are produced. Where  $W$  represents the residual values the Newton-Raphson solver tends to zero. This forms the first  $2 \times N + 1$  equations that are solved in the Newton-Raphson solver:

$$\begin{aligned} W_0 &= (\mathbf{Q})_{u,p}\bar{X}_0 + (\mathbf{Q})_{u,v}X_0 + (\mathbf{q}_n)_u F_0 \\ W_{k,s} &= -k^2\omega^2 X_{k,s} - (\mathbf{Q})_{u,p}\bar{X}_{k,s} + (\mathbf{Q})_{u,u}k\omega X_{k,c} - (\mathbf{Q})_{u,v}X_{k,s} - (\mathbf{q}_n)_u F_{k,s} \\ W_{k,c} &= -k^2\omega^2 X_{k,c} - (\mathbf{Q})_{u,p}\bar{X}_{k,c} + (\mathbf{Q})_{u,u}k\omega X_{k,s} - (\mathbf{Q})_{u,v}X_{k,c} - (\mathbf{q}_n)_u F_{k,c} \end{aligned} \quad (11)$$

Including the continuation parameter and natural frequency there is  $2 \times N + 3$  unknowns, so two more residual equations must be derived, which will be detailed in the following two subsections.

### 2.3.4 Continuation Constraint

A constraint can be defined based on pseudo-arclength continuation, allowing for another residual equation to be derived. Figure 2 shows the process of a tangent prediction being corrected through pseudo-arclength continuation. Predicted point  $j + 1$  is made using known the known  $j^{th}$  point and direction vector  $\frac{dX}{ds}$ , as well as a small arclength distance  $\delta s$ . The predicted  $j + 1, 0$  value is then corrected assuming the converged  $j + 1$  value is perpendicular to the initial prediction. As the dot product of perpendicular vectors is zero, in the case of the Fourier coefficients it can be assumed:

$$\left( \frac{X_{j+1} - X_{j+1,0}}{\delta s} \right) \cdot \frac{dX}{ds} = 0$$

Expanding for all system unknowns the residual Equation 12 can be written.

$$W_{2l+2} = (X_{j+1} - X_{j+1,0}) \frac{dX}{ds}_j + (\omega_{j+1} - \omega_{j+1,0}) \frac{d\omega}{ds}_j + (\lambda_{j+1} - \lambda_{j+1,0}) \frac{d\lambda}{ds}_j \quad (12)$$

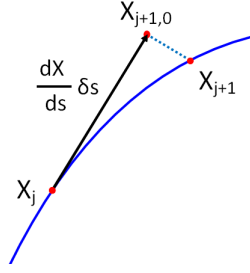


Figure 2: Pseudo-arclength continuation scheme

### 2.3.5 Phase Constraint

A final residual equation can be derived related to a phase constraint. It is common practice in continuation to assume orthogonality between a response and its differential. This assumption can be used to derive a relationship between  $j^{\text{th}}$  Fourier coefficients and the  $j + 1$  points in the 'Orthogonality Phase Condition' [25]:

$$\int_0^T \dot{x}(t)_j x(t)_{j+1} dt = 0$$

Or:

$$\mathbf{E}_j^T X_{j+1} = 0 \quad (13)$$

Where  $E_j^T = [0, -kX_{k,c}, kX_{k,s}]$  for  $k = 1, \dots, l$ .

Carrying out the integration and making use of Equations 5, the final residual Equation 14 is obtained.

$$W_{2l+3} = \sum_{k=1}^l -k(X_{k,c})_j (X_{k,s})_{j+1} + k(X_{k,s})_j (X_{k,c})_{j+1} \quad (14)$$

### 2.3.6 Residual Equations

With  $2l + 3$  residual equations matching the number of system unknowns  $[X_0, X_{k,s}, X_{k,c}, \omega, \lambda]$  (for  $k = 1, \dots, l$ ), the Newton-Raphson solver can be set up. System 15 shows the iterative process employed until a converged solution has been reached. Finite difference method is used to obtain the derivatives  $\frac{\delta W}{\delta X}$ ,  $\frac{\delta W}{\delta \omega}$  and  $\frac{\delta W}{\delta \lambda}$ .

$$\begin{pmatrix} X_{j+1,1} \\ \omega_{j+1,1} \\ \lambda_{j+1,1} \end{pmatrix} = \begin{pmatrix} X_{j+1,0} \\ \omega_{j+1,0} \\ \lambda_{j+1,0} \end{pmatrix} - \begin{bmatrix} \frac{\delta W}{\delta X}_{j+1} & \frac{\delta W}{\delta \omega}_{j+1} & \frac{\delta W}{\delta \lambda}_{j+1} \\ \frac{dX}{ds}_j^T & \frac{d\omega}{ds}_j & \frac{d\lambda}{ds}_j \\ \mathbf{E}^T & 0 & 0 \end{bmatrix}^{-1} \begin{pmatrix} W_{j+1,0} \\ W_{2l+2} \\ W_{2l+3} \end{pmatrix} \quad (15)$$

### 2.3.7 Calculation of Direction Vectors

Once a converged solution for all system unknowns is reached at  $j$ , calculation of  $j + 1$  direction vectors is carried out. It is commonly assumed in pseudo-arclength continuation that new direction vectors point the same direction as the previous ones:

$$\frac{dX}{ds}_j^T \frac{dX}{ds}_{j+1} = 1$$

As arcpoint  $s$  lies on the same curve created by solutions of  $W(X_0, X_{k,s}, X_{k,c}, \omega, \lambda) = 0$  for all values of  $s$  it can be said:

$$\frac{\delta W}{\delta X} \frac{dX}{ds} + \frac{\delta W}{\delta \omega} \frac{d\omega}{ds} + \frac{\delta W}{\delta \lambda} \frac{d\lambda}{ds} = 0$$

This principal is employed to construct the relationship in Appendix A.2. Allowing  $j + 1$  direction vectors to be obtained.

### 2.3.8 Stability Analysis

When applying HBM, solutions can converge to both stable and unstable states. A stable LCO solution describes behaviour where following an initial perturbation the response of a system is drawn towards the LCO. With an unstable LCO, the opposite is true and following a perturbation the response is a trajectory away from the unstable cycle [26]. Stability of a LCO can be computed in the frequency domain with Hill's method. Hill's method implements Floquet theory in the frequency domain [26]. Lazarus and Thomas demonstrate the accuracy of the method on a forced duffing oscillator system in Ref. [20]. Stability is computed based on the eigensolution of the truncated Hill's matrix  $\mathbf{H}$  as follows:

$$\mathbf{H} = \begin{bmatrix} \ddots & \vdots & \vdots & \vdots & \ddots \\ \dots & \mathbf{J}^0 + i\omega\mathbf{I} & \mathbf{J}^{-1} & \mathbf{J}^{-2} & \dots \\ \dots & \mathbf{J}^1 & \mathbf{J}^0 & \mathbf{J}^{-1} & \dots \\ \dots & \mathbf{J}^2 & \mathbf{J}^1 & \mathbf{J}^0 + i\omega\mathbf{I} & \dots \\ \ddots & \vdots & \vdots & \vdots & \ddots \end{bmatrix} \quad (16)$$

where  $\mathbf{J}^k$  is the Jacobian matrix related to the  $k^{\text{th}}$  harmonic. Natural frequency of the LCO is given by  $\omega$  and  $\mathbf{I}$  is an identity matrix of appropriate size.  $\mathbf{H}$  is truncated to a matrix of size  $N(2l + 1) \times N(2l + 1)$ . Eigenvalues  $\psi_n^l$  and eigenvectors  $\phi_n^l$  of  $\mathbf{H}$  associated to  $l = 0$  are selected by considering that  $\phi_n^0$  is the set of eigenvectors with the most symmetric shapes. The associated eigenvalues are then compared to zero to determine the periodic stability. This process is carried out at every converged solution in the continuation and the stability data is stored.

## 3 CASE STUDY

The methods detailed in the previous section are demonstrated on an aeroelastic test case. A freeplay nonlinearity is introduced to demonstrate the process's capability with non-smooth nonlinearities that are encountered in real aeroelastic systems. Freestream velocity  $U$  is taken as the continuation parameter due to its link to flutter behaviour. In this part, the model setup and nonlinearities is firstly described. Linear analysis is then conducted to determine the location of any hopf bifurcation points. The post-critical LCO behaviour is then tracked through the continuation methods described previously. Results are verified by comparing the displayed behaviour to time histories and the LCO plot to results from MATCONT and COCO. The accuracy and efficiency of the HBM is compared to the alternatives and discussed. The implications that nonlinear analysis has on design specifications is compared to purely linear analysis and highlighted to show benefits of including nonlinearities at early design stages.

### 3.1 Model Setup

The model investigated here is a two-degree-of-freedom aerofoil section shown in Figure 3. This is a simplified model of the system investigated in Ref. [27]. Pitch angle  $\theta$  and plunge  $z$  are the degrees of freedom. Plunge degree-of-freedom is constricted by a spring of stiffness  $K_z$

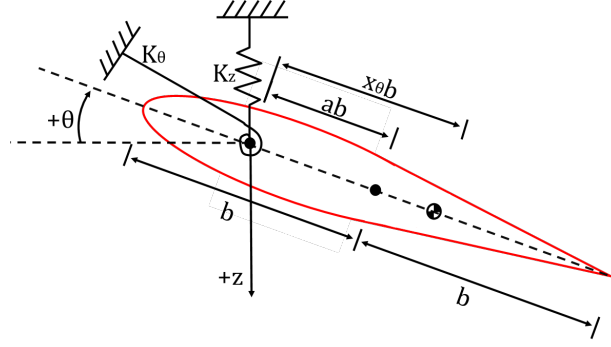
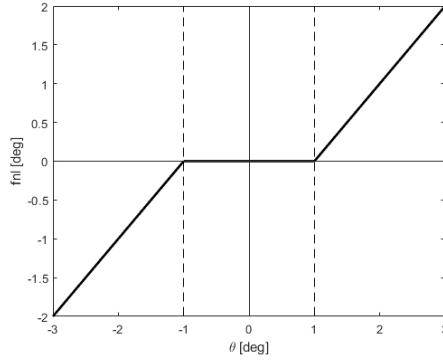


Figure 3: Freebody diagram of 2 DoF aerofoil


 Figure 4: Freeplay nonlinearity with  $\delta = 1^\circ$ 

and a torsional spring  $K_\theta$  resists pitch movement. A freeplay structural nonlinearity was added on the torsional spring, represented by Figure 4. This describes behaviour where between pitch angles of  $-\delta$  and  $\delta$ , the torsional stiffness is zero. The region of zero torsional stiffness is known as the freeplay region. Equations of motion can be derived from first principals as Equations 17. Effective pitch angle experienced by the torsional spring is taken as the nonlinear function  $f_{nl}(\theta)$  and is also expressed.

$$\begin{aligned} I_\theta \ddot{\theta} + S_\theta \ddot{z} + K_\theta f_{nl}(\theta) &= M_\theta \\ S_\theta \ddot{\theta} + M_w \ddot{z} + K_z z &= L \end{aligned} \quad (17)$$

Where  $I_\theta$  is the moment of inertia,  $S_\theta$  is the static moment of the wing and  $M_w$  is the mass of the wing. Aerodynamic forces are given by  $L$  and  $M_\theta$  and the nonlinear force is:

$$f_{nl}(\theta) = \begin{cases} \theta + \delta & \theta \leq -\delta \\ 0 & -\delta < \theta < \delta \\ \theta - \delta & \theta \geq \delta \end{cases}$$

Structural mass, stiffness and damping matrices  $M$ ,  $K$  and  $D$  are derived in Appendix B. Aerodynamic forces for an incompressible flow were taken from Ref. [28] to model aerodynamic moment  $M_\theta$  and lift  $L$ .

$$\begin{aligned} M_\theta &= -\rho b^2 \left\{ \pi \left( \frac{1}{2} - a \right) U b \dot{\theta} + \pi b^2 \left( \frac{1}{8} + a^2 \right) \ddot{\theta} - a \pi b \ddot{z} \right\} + 2\rho U b^2 \pi \left( a + \frac{1}{2} \right) C(k) \left\{ U \theta + \dot{z} + b \left( \frac{1}{2} - a \right) \dot{z} \right\} \\ L &= -\rho \pi b^2 \left( U \dot{\theta} + \ddot{z} - b a \ddot{\theta} \right) - 2\pi \rho U b C(k) \left\{ U \theta + \dot{z} + b \left( \frac{1}{2} - a \right) \dot{\theta} \right\} \end{aligned} \quad (18)$$

Where  $C(k)$  is the generalised Theodorsen's function detailed in again in Ref. [28]. Theodorsen's function is related to the model through reduced frequency  $k$  that can be calculated with  $k = \omega b/U$ . Aerodynamic mass, damping and stiffness matrices (A,B,C) can now be derived:

$$\begin{aligned}
 A &= \rho\pi b^2 \begin{bmatrix} -b(\frac{1}{8} + a^2) & ba \\ ba & -1 \end{bmatrix} \\
 B &= \rho\pi bU \begin{bmatrix} -b^2(\frac{1}{2} - a) & 2bC(k)(a + \frac{1}{2})(1 + b(\frac{1}{2} - a)) \\ -b(1 + 2C(k)(\frac{1}{2} - a)) & -2C(k) \end{bmatrix} \\
 C &= 2\rho\pi bU^2 C(k) \begin{bmatrix} b(a + \frac{1}{2}) & 0 \\ 1 & 0 \end{bmatrix}
 \end{aligned}$$

The aerodynamic forces and structural matrices are combined in the generalised form from Equation 2. With the nonlinearity in the pitch degree-of-freedom, the Boolean matrix to allocate the nonlinear function can be defined as  $q_n = [1, 0]^T$ . This allows linear flutter analysis to take place followed by the numerical continuation method detailed.

Table 1: Parameters used in case study

Parameter	Value
$c$	$0.254m$
$b$	$0.127m$
$a$	$-0.5$
$M_w$	$0.62868kg$
$m$	$1.558kg$
$S_\theta$	$0.08587kg.m$
$x_\theta$	$0.434$
$I_\theta$	$0.01347kgm^2$
$K_\theta$	$37.3kg/s^2$
$K_z$	$2818.8N/m$
$\zeta_1$	$0.01626$
$\zeta_2$	$0.0113$

### 3.2 Linear and LCO Analysis

Using parameters in Table 1, it was found that the linear flutter velocity without torsional stiffness was  $31.45m/s$  and with was  $29.5m/s$ . A successful continuation was run from the hopf point at  $31.45m/s$  using the proposed HBM solver. Figure 5a. shows the maximum point of the resultant LCO detected at varying airspeed. It is observed that multiple solutions exist between airspeeds of  $24.3m/s$  and  $29.5m/s$  and vibration responses exist before the linear flutter speed. Figure 5b. also shows LCO development with different orders of harmonics. It is observed that the harmonic order impacts the location of the turning point. With lower harmonic orders the turning point appears occur at lower velocities. Table 2 shows a convergence of results at  $l = 8$  when comparing the location of the turning point to the harmonic order of the system.

Stability analysis was implemented once a converged solution had been reached. It is shown in Figure 5a. that unstable LCO are formed at the bifurcation point and continue backwards with respect to velocity to  $24.2m/s$ . A turning point is then reached where there is an exchange of stability. Stable LCO of increasing amplitude are then formed from  $24.3m/s$  until  $29.5m/s$ . This is the standard linear flutter speed with no freeplay nonlinearity included. At  $29.5m/s$  flutter behaviour is observed, where the amplitude of the LCO tend to infinity.

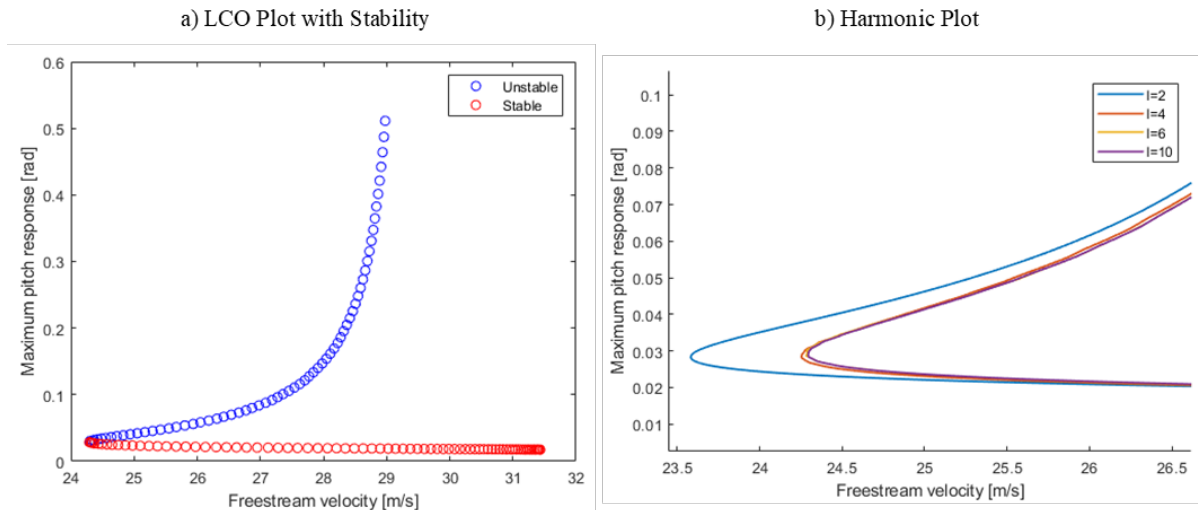


Figure 5

 Table 2: Freestream velocity turning point occurs  $[m/s]$  in relation to  $l$ .

$l$	1	2	3	4	5	6	7	8	9
$U_{TP}$	23.5827	23.5827	24.2532	24.2532	24.2801	24.2801	24.29	24.29	24.29

### 3.3 Result Validation

A comparison between the LCO plot and time histories gathered from the *ode45* differential equation solver in MATLAB is shown in Figure 6. This figure demonstrates the physical significance of the LCO plot, as well as validating the accuracy. At velocities lower than the turning point, the response of the system to any initial perturbation in pitch or plunge is to oscillate with positive damping before settling to a steady rest state at zero. Responses at velocities between the turning point and linear flutter speed with torsional stiffness are dependant on the magnitude of the initial perturbation. Low perturbations exhibit behaviour similar to the response below the turning point. With larger perturbations in pitch, LCO are generated. Figure 6 shows that the maximum point of the time responses accurately corresponds to the curve generated from the HBM results. Beyond  $29.5m/s$  until  $31.45m/s$  the LCO plot shows unstable LCO that either push the response to a stable solution, or away towards infinity. This is validated from the time responses, as with low perturbations the systems settles and with larger ones the system is dynamically unstable in Figure 6. Above the linear flutter speed without torsional stiffness, it is shown in both the LCO plot and the time histories no stable solutions exist and the response to any perturbation is binary flutter. It is observed here that the amplitude of the unstable section of the LCO plot does not hold physical significance. What is shown is that solutions lie either side of the branch, in this case either settling to rest at a steady state or a vibrational response (flutter or a LCO).

When comparing the results to MATCONT and COCO a high level of accuracy is observed. Figure 7 show that prediction of the amplitude of the stable LCO is accurate. Inaccuracies exist in the amplitude of the unstable region as is shown in Figure 7 and Table 3. At the hopf point the amplitude error is at 45.71%. By  $27m/s$  the sets of data are in agreement. Both MATCONT and COCO agree on the amplitude of LCO at low pitch inputs, indicating this inaccuracy comes from HBM. Figure 8 shows that at  $l = 8$  when it appears the results have converged the nonlinear force response is not fully captured. With HBM, the peak of the true

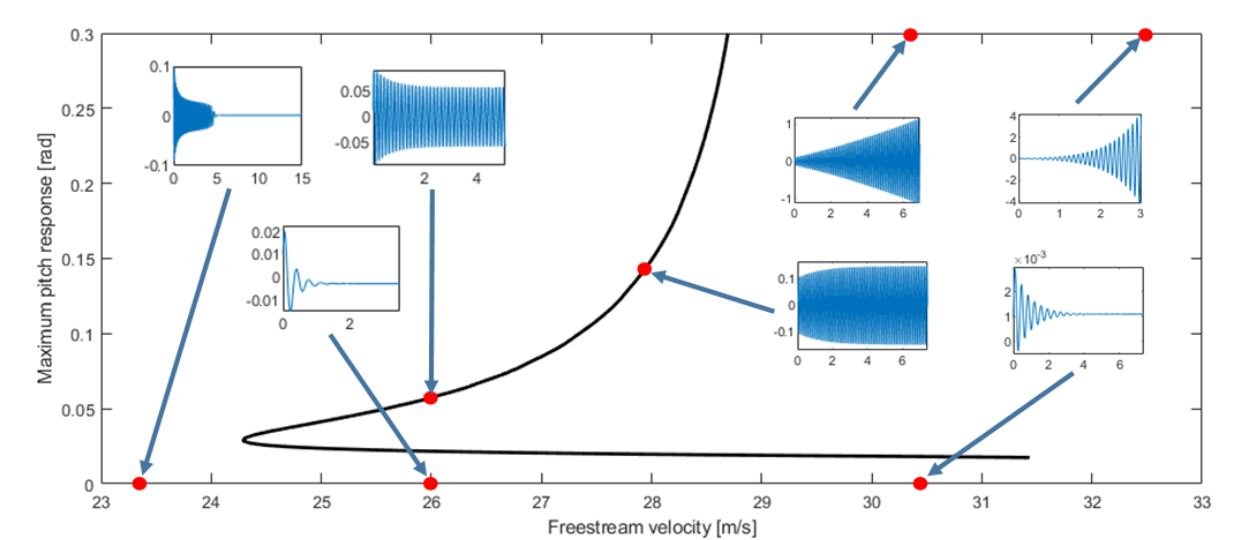


Figure 6: Comparison of bifurcation plot with time histories

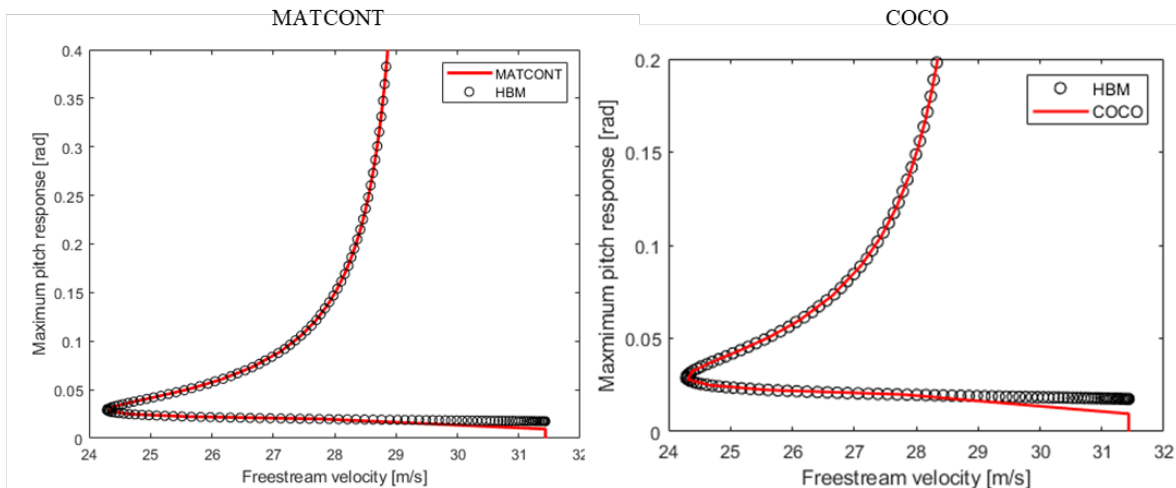


Figure 7: Comparison of bifurcation results with alternative software

nonlinear force is not reached at low inputs of pitch at  $30\text{ m/s}$ . Between pitch inputs of  $-\delta$  and  $\delta$ , HBM response oscillates around zero instead of maintaining absolute zero. The inaccuracy becomes less pronounced as the size of the inputs is increased. This source of error has been described by Gibbs phenomenon [29]. It is stated that the error will reduce as the number of harmonics is increased but always be present to some degree [30].

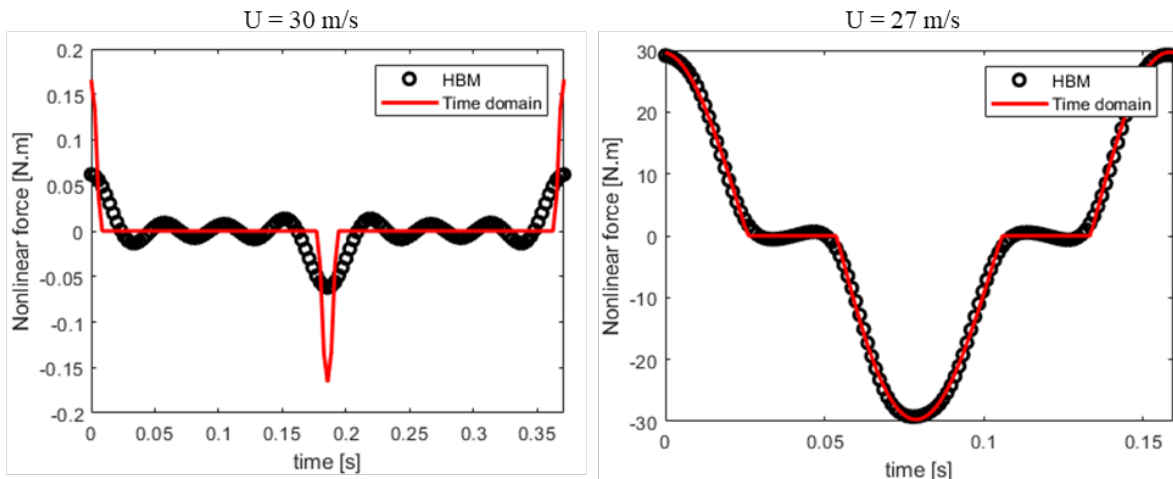
Table 3: Discrepancy in data for low inputs of pitch comparing HBM to MATCONT

$U$ [m/s]	31.43	31	30.5	30	29.5	29	28.5	28	27.79	27.5
Error [%]	45.71	40.56	33.31	24.44	16.67	13.10	5.26	2.18	0.54	0.23

A comparison of running times and data points required is shown in Table 4. When comparing HBM to MATCONT, it is observed that for a converged solution at  $l = 8$  HBM runs over 11 times faster. The data storage requirements of HBM are lower, requiring 97.79% less data be stored. The HBM at  $l = 8$  runs 3 times faster than COCO and also with 30% less data storage demands. As the harmonic orders of the analysis increases, HBM has higher data storage

Table 4: HBM time and data storage requirement comparison with alternative software to run continuation for  $j = 150$ . Data storage represents the number of data points gathered from the full continuation

Software	Run Time [s]	Data Storage
HBM( $l = 5$ )	14.819	2250
HBM( $l = 8$ )	19.039	3150
HBM( $l = 15$ )	35.876	5250
MATCONT	215.97	96900
COCO	55.746	4650


 Figure 8: Nonlinear force response at  $l = 8$ 

demands than COCO as it is shown with  $l = 15$ . In this test case, with accurate fully converged results ( $l = 8$ ) both the run time and data storage requirement favour HBM. Considering stability analysis, MATCONT does not provide stability analysis for LCO. COCO predicted an exchange of stability at the turning point, in the same location as the implemented Hill's method.

### 3.4 Design Implications

From a design perspective nonlinear analysis results have significant implications. Using typical linear aeroelastic analysis it would appear the system is safe until the flutter speed is reached at  $31.5$  m/s. However, when including a single nonlinearity in the analysis it is found that potentially unsafe vibrational responses exist 18% below the linear flutter speed at  $24.5$  m/s. Figure 9 demonstrates this unsafe region displaying the amplitude of the resulting LCO. At low pitch disturbances it is also shown from nonlinear analysis that the system is stable 6% past the linear flutter speed.

## 4 CONCLUSION

A tool was developed capable of modelling both the stable and unstable LCO behaviour of nonlinear aeroelastic systems based around HBM. From the low degree of freedom case study carried out, results produced are promising. Comparison of HBM results with time histories proved the method is capable of representing the physical behaviour of nonlinear systems. A series of time histories for different initial perturbations is not required from the HBM making it a far more computationally efficient method. Also the LCO plot is capable of representing multiple solutions at a single point in  $\lambda$ . In the comparison with MATLAB and COCO, HBM continuation proved to run faster than the two alternatives and with less data storage require-

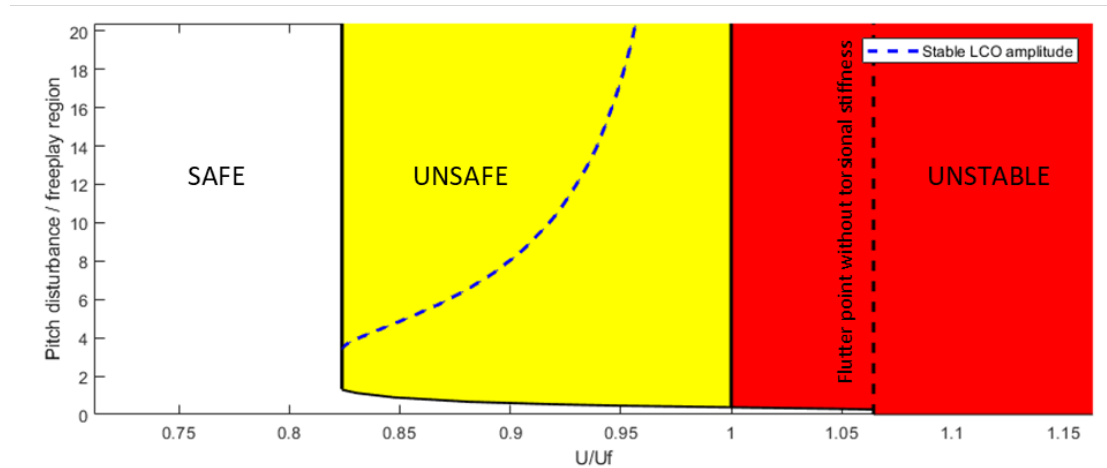


Figure 9: Impact of freeplay nonlinearity on design

ments. This accounted for an 11 times speed up compared to MATCONT and a 3 times with COCO. There was a slight loss of accuracy with low pitch inputs converting the nonlinear force from the time domain to the frequency domain in the AFT procedure. This inaccuracy was only present in the amplitude of the unstable LCO for this case study. Unstable LCO do not represent a solution that the system will settle to, so the amplitude on the LCO diagram does not hold a great deal of physical significance. The purpose of the unstable branch is to represent that multiple solutions exist on either side of the branch. Benefits of including nonlinearities in the design process was also demonstrated. With purely linear aeroelastic analysis of the case study, the design appears dynamically stable in areas where it is shown from nonlinear analysis potentially unsafe LCO exist. This unsafe region extends to an airspeed 18% lower than the flutter speed meaning the safety region of the design is overestimated. While the results from this case study are promising, further work on the method is required. Improving the accuracy of HBM at low inputs is necessary. This could potentially be achieved through performing HBM with high levels of harmonics at low inputs to the nonlinear force and reducing the level of Harmonic with larger inputs to improve efficiency. However, this may be challenging as this inaccuracy is the limitation of HBM itself. The capability of developed tool at handling systems with sources of nonlinearities in multiple degrees and with higher degrees of freedom must also be tested.

## 5 ACKNOWLEDGEMENTS

M.McGurk acknowledges the support of EPSRC Doctoral Training Partnership studentship. J. Yuan acknowledges the support of Research Grant and Saltire Workshop Awards from Royal Society of Edinburgh.

## 6 APPENDIX

### A HBM CONSTRUCTION

#### A.1 Reduced Newton-Raphson solver

Detailed is the reduced Newton-Raphson solver that is used to obtain points  $j = 0$  and  $j = 1$ , initiating continuation.

$$\begin{pmatrix} \delta X \\ \delta \omega \end{pmatrix} = - \left[ \begin{array}{cc} \frac{\delta W^*}{\delta X_{j+1}} & \frac{\delta W}{\delta \omega_{j+1}} \end{array} \right]^{-1} (W_{j+1,0})$$

$$\begin{pmatrix} X_{j+1,1} \\ \omega_{j+1,1} \end{pmatrix} = \begin{pmatrix} X_{j+1,0} \\ \omega_{j+1,0} \end{pmatrix} + \begin{pmatrix} \delta X \\ \delta \omega \end{pmatrix}$$

Where  $\frac{\delta W^*}{\delta X}$  is the same as  $\frac{\delta W}{\delta X}$  but with the term related to  $X_{1,s}$  removed as it is treated as a known.

## A.2 Direction vector solver

Shown is the system employed to obtain  $j + 1$  direction vectors based on  $j^{th}$  direction vectors and  $j + 1$  Jacobi.

$$\begin{pmatrix} \frac{dX^T}{ds}{}_{j+1} \\ \frac{d\omega}{ds}{}_{j+1} \\ \frac{dU}{ds}{}_{j+1} \end{pmatrix} = \begin{bmatrix} \frac{\delta W}{\delta X}{}_{j+1} & \frac{\delta W}{\delta \omega}{}_{j+1} & \frac{\delta W}{\delta U}{}_{j+1} \\ \frac{dX^T}{ds}{}_{j+1} & \frac{d\omega}{ds}{}_{j+1} & \frac{dU}{ds}{}_{j+1} \\ \mathbf{E}^T & 0 & 0 \end{bmatrix}^{-1} \begin{pmatrix} 0 \\ 1 \\ 0 \end{pmatrix} \quad (19)$$

## B AEROFOIL MODEL STRUCTURAL MATRICES

### B.1 Nondimensional relationships

The following relationships are utilised in converting Equations 17 to nondimensional form and then derive the structural mass stiffness and damping matrices.

$$\bar{M}_\theta = \frac{M_\theta}{mb^2} \qquad \bar{L} = \frac{L}{mb}$$

$$r_\theta = \sqrt{\frac{I_\theta}{mb^2}} \qquad x_\theta = \sqrt{\frac{S_\theta}{mb}} \qquad \omega_\theta = \sqrt{\frac{K_\theta}{I_\theta}} \qquad \omega_z = \sqrt{\frac{K_z}{m}}$$

Where  $b$  is the semichord and  $m$  is mass per unit length of the wing. Equation 17 to nondimensional form:

$$\begin{aligned} r_\theta^2 \ddot{\theta} + x_\theta \ddot{z} + r_\theta^2 \omega_\theta^2 f_{nl}(\theta) &= \bar{M}_\theta \\ x_\theta \ddot{\theta} + \frac{M_T}{m} \ddot{z} + \omega_z^2 z &= \bar{L} \end{aligned} \quad (20)$$

From the nondimensional equations of motion, structural mass, damping and stiffness matrices are derived.

$$M = \begin{bmatrix} r_\theta^2 & x_\theta \\ x_\theta & M_w/m \end{bmatrix} \qquad K = \begin{bmatrix} r_\theta^2 \omega_\theta^2 & 0 \\ 0 & \omega_z^2 \end{bmatrix} \quad (21)$$

### B.2 Structural damping matrix derivation

Then structural damping matrix  $D$  is found using the relationship:

$$D = (\Lambda^T)^{-1} D_{mod} \Lambda$$

Where  $\Lambda$  is the eigenvectors of the system  $M\ddot{\mathbf{x}} + K\mathbf{x} = 0$ ,  $\psi_i$  being the corresponding eigenvalues, and:

$$D_{mod} = \begin{bmatrix} 2m_1\omega_1\zeta_1 & 0 \\ 0 & 2m_2\omega_2\zeta_2 \end{bmatrix}$$

With  $\zeta_i$  the measured damping ratios,  $\omega_i$  the coupled natural frequencies and  $m_i$  the modal masses. Natural frequencies are found with  $\omega_i = \sqrt{\psi_i}$ . Modal masses are obtained from the diagonal of  $M_{mod}$ , where:

$$M_{mod} = \Lambda^T M \Lambda$$

**C REFERENCES**

- [1] Howcroft, C., Lowenberg, M., Neild, S., et al. (2015). *Shimmy of an Aircraft Main Landing Gear with Geometric Coupling and Mechanical Freeplay*. Journal of Computational and Nonlinear Dynamics. 10(5).
- [2] Masarati, P., Piatak, D., and Quaranta, G. (2008). *Soft-inplane tiltrotor aeromechanics investigation using two comprehensive multibody solvers*. J. Am. Helicopter Soc.
- [3] Phillips, W., Alley, N., and Niewoehner, R. (2008). *Effects of Nonlinearities on Subsonic Aerodynamic Center*. Journal of Aircraft - J AIRCRAFT. 45. 1244-1255. 10.2514/1.34241.
- [4] Mair, C. (2021). *Stability Analysis of Whirl Flutter in Rotor-Nacelle Systems with Structural Nonlinearities*. The University of Bristol.
- [5] Edenborough, H. (1968). *Investigation of Tilt-Rotor VTOL Aircraft Rotor-Pylon Stability*. Journal of Aircraft. 5(6).
- [6] Seydel, R. (2009). *Practical Bifurcation and Stability Analysis*. 3rd edn. Springer. Pp75-77.
- [7] Guckenheimer, J. and Holmes, P. (2013). *Nonlinear oscillations, dynamical systems, and bifurcations of vector fields*. Springer.
- [8] Tartaruga, I., Barton, D., Rezgui, D., et al. (2019). *Experimental bifurcation analysis of a wing profile*. Conference: International Forum on Aeroelasticity and Structural Dynamics : IFASD 2019.
- [9] Detroux, T., Renson, L., Masset, L., et al. (2016). *The Harmonic Balance Method for Bifurcation Analysis of Nonlinear Mechanical Systems*. In: Kerschen G. (eds) Nonlinear Dynamics, Volume 1. Conference Proceedings of the Society for Experimental Mechanics Series. Springer, Cham. <https://doi.org/10.1007/978-3-319-15221-95>.
- [10] Blyth, M., Renson, L., and Marucci, L. (2020). *Tutorial of numerical continuation and bifurcation theory for systems and synthetic biology*. Unpublished. <https://arxiv.org/abs/2008.05226>.
- [11] Karkar, S., Cochelin, B., and Vergez, C. (2014). *A comparative study of the harmonic balance method and the orthogonal collocation method on stiff nonlinear systems*. Journal of Sound and Vibration. Volume 333, Issue 12, pp2554-2567. ISSN 0022-460X.
- [12] Annick, D., W., G., Kuznetsov, Y., et al. (2008). *New features of the software matcont for bifurcation analysis of dynamical systems*. *Mathematical and Computer Modelling of Dynamical Systems*. 14(2):147–175.
- [13] Doedel, E. and Oldeman, B. (2009). *AUTO-07P: Continuation and Bifurcation Software for Ordinary Differential Equations*. Concordia University, Montreal, Canada.
- [14] Dankowicz, H. and Schilder, F. (2013). *Recipes for continuation*. volume 11. SIAM.
- [15] Gudmundson, P. (1989). *On The Accuracy Of The Harmonic-Balance Method Concerning Vibrations Of Beams With Nonlinear Supports*. *Archive of Applied Mechanics*. (1991) 59:5, p. 333-344.

- [16] Razzak, M. (2016). *A simple harmonic balance method for solving strongly nonlinear oscillators*. Journal of the Association of Arab Universities for Basic and Applied Sciences. 21:1, 68-76, DOI: 10.1016/j.jaubas.2015.10.002.
- [17] Lanza, V., Bonnin, M., and Gilli, M. (2007). *On the application of the describing function technique to the bifurcation analysis of nonlinear systems*. Circuits and Systems II: Express Briefs. IEEE Transactions on, vol. 54, no. 4, pp. 343–347.
- [18] Krack, M. and Groß, J. (2020). *NLvib*. University of Stuttgart. Available at: NLvib — Institut für Luftfahrtantriebe — Universität Stuttgart (uni-stuttgart.de) (Accessed 10/12/2021).
- [19] Cameron, T. and Griffin, J. (1989). *An Alternating Frequency/Time Domain Method for Calculating the Steady-State Response of Nonlinear Dynamic Systems*. Journal of Applied Mechanics. American Society of Mechanical Engineers, ff10.1115/1.3176036ff. fihal-01333697.
- [20] Lazarus, A. and Touzé, C. (2010). *A Harmonic-Based Method for Computing the Stability of Periodic Oscillations of Non-Linear Structural Systems*. Proceedings of the ASME Design Engineering Technical Conference. 5. 10.1115/DETC2010-28407.
- [21] Lazarus, A. and Thomas, O. (2010). *A harmonic-based method for computing the stability of periodic solutions of dynamical systems*. Comptes Rendus Mécanique. ”Volume 338, Issue 9, 2010, Pages 510-517, ISSN 1631-0721.
- [22] Abdelkefi, A., Vasconcellos, R., Marques, F., et al. (2012). *Modeling and identification of freeplay nonlinearity*. Journal of Sound and Vibration. Volume 331, Issue 8, Pages 1898-1907, ISSN 0022-460X.
- [23] Dimitriadis, G. (2017). *Introduction to Nonlinear Aeroelasticity*. Chichester: John Wiley Sons Ltd.
- [24] Wright, J. and Cooper, J. (2014). *Introduction to Aircraft Aeroelasticity and Loads*. 2nd edn. Chichester: John Wiley Sons Ltd. Chapter 10.4.
- [25] Govaerts, W. (2000). *Numerical bifurcation analysis for ODEs*. Journal of Computational and Applied Mathematics. 125(1–2), 57–68.
- [26] Peletan, L., Baguet, S., Torkhani, M., et al. (2013). *A comparison of stability computational methods for periodic solution of nonlinear problems with application to rotordynamics*. Nonlinear Dynamics. 72. 671-682. 10.1007/s11071-012-0744-0.
- [27] Liu, L. and Dowell, E. (2005). *Harmonic Balance Approach for an Airfoil with a Freeplay Control Surface*. Aiaa Journal - AIAA J. 43. 802-815. 10.2514/1.10973.
- [28] Theodorsen, T. (1935). *General Theory of Aerodynamic Instability and the Mechanism of Flutter*. NACA Rept. 496.
- [29] Hewitt, E. and Hewitt, R. (1979). *The Gibbs-Wilbraham Phenomenon: An Episode in Fourier Analysis*. Springer-Verlag. Archive for History of Exact Sciences, Volume 21.
- [30] Carslaw (1930). *Introduction to the theory of Fourier’s series and integrals (Third ed.)*. New York: Dover Publications Inc.

## **COPYRIGHT STATEMENT**

The authors confirm that they, and/or their company or organization, hold copyright on all of the original material included in this paper. The authors also confirm that they have obtained permission, from the copyright holder of any third party material included in this paper, to publish it as part of their paper. The authors confirm that they give permission, or have obtained permission from the copyright holder of this paper, for the publication and distribution of this paper as part of the IFASD-2022 proceedings or as individual off-prints from the proceedings.